Short Communications

Performance comparison of photodynamic antimicrobial chemotherapy with visible-light-activated organic dyes: Rose bengal, crystal violet, methylene blue, and toluidine blue O

Jae Hak Shin[a, †], Sang Bin Jeong[a,b, †], In Ho Kim[a], Seung Yeon Lee[a], Gi Byoung Hwang[c], Inyong Park[d], Ki Joon Heo[e,*], and Jae Hee Jung[a,*]

[a] Department of Mechanical Engineering, Sejong University, Seoul 05006, Republic of Korea

[b] Indoor Environment Center, Korea Testing Laboratory, Seoul 08389, Republic of Korea

[c] Material Chemistry Research Centre, Department of Chemistry, University College London, London WC1H 0AJ, United Kingdom

[d] Department of Environmental Machinery, Korea Institute of Machinery and Materials, Daejeon 34141, Republic of Korea

[e] Department of Mechanical Engineering, Chonnam National University, Gwangju 61186, Republic of Korea

† These authors contributed equally to this work.

*Corresponding authors. *E-mail* address: jaehee@sejong.ac.kr (J.H. Jung), k.heo@jnu.ac.kr (K.J. Heo)

Abstract

This study evaluated the photobiocidal performance of four widely distributed visible-light-activated (VLA) dyes against two bacteria (*Staphylococcus epidermidis* and *Escherichia coli*) and two bacteriophages (phages MS2 and phi 6): rose bengal (RB), crystal violet, methylene blue, and toluidine blue O (TBO). The photobiocidal performance of each dye depended on the relationship between the type of dye and microorganism. Gram-negative *E. coli* and the non-enveloped structure of phage MS2 showed more resistance to the photobiocidal reaction than Gram-positive *S. epidermidis* and the enveloped structure of phage phi 6. RB had the highest potential to yield reactive oxygen species. However, the photobiocidal performance of RB was dependent on the magnitude of the surface charge of the microorganisms; for example, anionic RB induced a negative surface charge and thus electrical repulsion. On the other hand, the photobiocidal performance of TBO was observed to be less affected by the microorganism type. The comparative results presented in our study have significant implications for selecting photodynamic antimicrobial chemotherapy (PACT) dyes suitable for specific situations and purposes. Furthermore, they contribute to the advancement of PACT-related technologies by enhancing their applicability and scalability.

Keywords

Photodynamic antimicrobial chemotherapy (PACT); Visible-light-activated; Organic dyes; Antimicrobial; Bactericidal; Virucidal

Introduction

Microbial threats pose some of the most severe and escalating problems in healthcare today. In particular, the phenomenon of antimicrobial resistance (AMR) is raising serious concerns. AMR microbes, including methicillin-resistant *Staphylococcus aureus* and multidrug-resistant tuberculosis, cause approximately 700,000 casualties worldwide each year (O'Neill, 2016), and were responsible for 1.3 million deaths in 2019 (Murray et al., 2022). Accordingly, the World Health Organization has also recognized this risk and declared AMR as one of the top 10 global public health threats facing humanity (Kumar, 2021). Therefore, countermeasures to build a safer medical environment against AMR are urgently needed.

Photodynamic therapy has been highlighted as a potential alternative to traditional antimicrobial treatments (Daniell and Hill, 1991; Hamblin and Hasan, 2004; Klausen et al., 2020). Photodynamic antimicrobial chemotherapy (PACT) utilizes light excitation of a nontoxic photosensitizer (PS) to produce reactive oxygen species (ROS), resulting in the death of microbial cells. (Castano et al., 2004; Daniell and Hill, 1991; Derosa and Crutchley, 2002). ROS are capable of multi-site attacks, allowing efficient non-selective inactivation without concerns about antibiotic resistance.

Because the efficacy of PACT against pathogens depends on the type and concentration of visible-light-activated (VLA) dyes, devising novel antimicrobial strategies requires substantial effort in selecting appropriate dyes. Numerous studies have evaluated PACT performance for various organic dyes. Rolim et al. evaluated the antimicrobial performance against *Streptococcus mutans* using different organic dyes, including methylene blue (MB), toluidine blue O (TBO), and rose bengal (RB) (Rolim et al., 2012). Soria-Lonazo et al. reported the performance of the PACT against cariogenic microorganisms using different organic dyes (Soria-Lozano et al., 2015). Moreover, Vilela et al. evaluated the photodynamic inactivation of *S. aureus* and *Escherichia coli* using MB and TBO (Vilela et al., 2012). However, because the dye activation conditions and target strains used in each study were all different, quantitative comparison of PACT performance is challenging. Indeed, more studies focusing on comparing PACT performance under constant conditions are needed to select a more appropriate VLA dye.

In this study, we carried out a quantitative comparison of the photobiocidal

performance of four VLA dyes under controlled photoactivation conditions: RB (a halogenated xanthene dye), crystal violet (CV; a triarylmethane dye), and MB and TBO (both phenothiazine dyes) (Figs. 1a-c). We quantified the performance of each at various concentrations against Gram-positive bacteria (*Staphylococcus epidermidis*) and Gram-negative bacteria (*E. coli*) as surrogates for AMR. In addition, an enveloped virus (phage phi 6) and a non-enveloped virus (phage MS2) were added as target microbes to meet the increased need for verification of biocidal performance against pathogenic viruses due to the Coronavirus 2019 (COVID-19) pandemic. We also determined the antimicrobial mechanisms of VLA dyes by tracking the changes in the physicochemical properties, such as the time-resolved photoluminescence decay and self-degradation rate. Our results can be used as a basis for selecting the optimal PACT dye for a specific purpose.

Materials and Methods

Preparation of an aqueous solution of VLA organic dyes

CV ($C_{25}H_{30}N_3Cl$, G2039); MB ($C_{16}H_{18}ClN_3S{\cdot}xH_2O$, M9140); RB ($C_{20}H_2Cl_4I_4Na_2O_5$, 330000); and TBO ($C_{15}H_{16}ClN_3S$, T3260) powders were purchased from Sigma-Aldrich (St. Louis, MO, USA). The dye solutions were prepared by dissolving each powder in deionized water (DIW) (Fig. 1d). The absorbance of the dyes was measured using a UV–Vis spectrophotometer (UV-2600i, Shimadzu, Kyoto, Japan). Figure 1e shows the absorbance spectra of the VLA dyes. The peak wavelengths for CV, MB, RB, and TBO were found at 591, 664, 549, and 633 nm, respectively. Despite the same concentrations, the dyes had varying maximum absorbance values due to their different molar absorption coefficients and chemical structures.

Preparation of microorganism suspensions

S. epidermidis, a Gram-positive bacterium (KCTC 1917; Korean Collection for Type Cultures), and *E. coli*, a Gram-negative bacterium (KCTC 1039), were used as the target bacteria. Each bacterium was incubated in a nutrient broth (0.3% beef extraction, 0.5% peptone; Becton Dickinson, Franklin Lakes, NJ, USA) at 37°C for 24 h until the suspension reached an optical density of 0.6 at 600 nm. The cultured bacteria were subsequently harvested by centrifugation (5000×g for 10 min) and washed in 10 mL

DIW to remove unwanted debris. All of the bacteria used in the experiment were serially diluted onto nutrient agar plates (0.3% beef extraction, 0.5% peptone, 1.5% agar; Becton Dickinson Franklin Lakes, NJ, USA), incubated at 37°C for 24 h, and then quantified in terms of colony-forming units (CFUs).

A non-enveloped phages MS2 and an enveloped phage phi 6 were used as target microbes. To prepare phage MS2, a host *E*. *coli* strain C3000 (ATCC 15597; American Type Culture Collection, Manassas, VA, USA) was incubated overnight at 37°C for 24 h using tryptic soy broth (TSB; Difco Laboratories, Detroit, MI, USA). Then, phage MS2 (ATCC 15597-B1) was dispersed in the host cell solution and incubated overnight at 37°C. To extract MS2, an equal volume of chloroform was added to the culture suspension and centrifuged at 4000×g for 20 min to remove the residue. The supernatant was collected and transferred to 10 mL TSB. A mixture of 0.1 mL MS2 and 0.3 mL the log-phase host *E*. *coli* C3000 was combined with 29.6 mL soft tryptic soy agar (TSA; Difco Laboratories), poured into Petri dishes, and incubated at 37°C until plaque was visible. Then, the concentration of phage MS2 was determined in terms of plaque-forming unit (PFU).

For the preparation of phage phi 6, host *Pseudomonas syringae* (DSM 21482; DSMZ-German Collection of Microorganisms and Cell Cultures GmbH, Braunschweig, Germany) was incubated overnight at 25°C until the optical density at 600 nm reached 0.3. A single plaque of phage phi 6 was dispersed in 100 µL SM buffer (100 mM NaCl, 10 mM $MgSO_4$, 50 mM Tris–HCl [pH 7.5], and 0.01% [w/v] gelatin) to infect the host *P*. *syringae*. The culture medium was incubated at 25°C until lysis occurred, centrifuged (4000×g for 20 min), and filtered through a 0.2 µm syringe filter (Minisart, Sartorius, Göttingen, Germany). For phage phi 6, a double-layer plaque assay was used. Petri dishes with a bottom agar layer (15 mL TSA) were prepared in advance. TSB with 0.75% agar, maintained at 48°C in a water bath, was used as the top agar layer. A well-mixed solution containing the log-phase host *P*. *syringae* (0.3 mL), phage phi 6 (0.5 mL), and the prepared TSB with 0.75% agar (14.2 mL) was poured over the bottom agar layer. The resulting plates were incubated at 25°C until the plaques became detectable. The concentrations of phages phi 6 were also determined by the PFU.

Evaluation of the photobiocidal efficacies of the VLA dyes

Figure 1f shows the schematic of the photobiocidal efficacy assessment. All target microbe suspensions were prepared in DIW. At this time, the concentrations of the *S. epidermidis* and *E. coli* suspensions were ~10^7 and ~10^8 CFU/mL, respectively. In addition, the concentrations of the suspensions of phages MS2 and phi 6 were ~10^8 and ~10^7 PFU/mL, respectively. The PS solutions of various concentrations were also prepared in DIW. Then, 0.5 mL of each prepared microbe suspension and the PS solution was loaded into a UV/Visible range cuvette. As a specific example, a 10 mM microbe-PS mixture was prepared by mixing 0.5 mL of 20 mM PS solution. The microbe-PS mixtures were subjected to dark or light exposure conditions for 4 h (Fig. 1g). Unless specified otherwise, the light exposure for the photobiocidal efficacy assessment was maintained at an intensity of 11.9 mW/cm^2 for 4 h. After exposure, the viable counts of the bacteria and bacteriophages were determined as the CFU and PFU concentrations, respectively.

Time-resolved fluorescence (TRF) measurement.

A TRF study was carried out using a confocal microscope (MicroTime-200, PicoQuant, Berlin, Germany). A single-mode pulsed diode laser (470 nm with a pulse width of ~30 ps and an average power of 10–100 μW, operating at a 40 MHz repetition rate) was used as an excitation source. A dichroic mirror (490 DCXR, AHF); long-pass filter (HQ500lp, AHF); and single-photon avalanche diode (PDM series, MPD) were used to collect the emissions from the samples. A time-correlated single-photon counting system (PicoHarp-300, PicoQuant) was used to count the emitted photons. Exponential function fitting for the obtained fluorescence decays was performed using the Symphotime-64 software (Ver. 2.2).

Assessment of the self-degradation rate of the VLA dyes

To evaluate the self-degradation rate of the VLA dyes, all of the dyes were prepared at the same concentration (10 μM) in a cuvette. The VLA dyes were exposed to a constant light power (11.9 mW/cm^2) for specific durations, and their self-degradation rates were subsequently compared by monitoring the absorbance values at their respective peak wavelengths.

Light exposure conditions

To evaluate both the photobiocidal performance and the rate of photo-induced degradation of the VLA dyes, a light-emitting-diode lamp (LVG95L 12W, LEDVANCE, Garching bei München, Germany) was utilized. Figure 1h shows the spectrum and optical power of the lamp. The spectrum was measured using a spectrometer (USB2000+; Ocean Optics, Orlando, FL, USA), and the optical power was measured with a power meter (PM400; Thorlabs, Newton, NJ, USA) and a thermal sensing position detector (S440C, Thorlabs). The optical power was regulated by adjusting the distance between the detector and light source. The optical powers recorded at 300, 100, and 50 mm were 1.0, 5.8, and 11.9 mW/cm^2, respectively. The experiment was carried out by positioning the test sample where the optical power could be measured accurately.

Results and Discussion

Figure 2 shows the photodynamic inactivation performance of VLA dyes. For *E. coli*, no significant bactericidal effects were observed under dark conditions up to a concentration of ~500 μM for all of the dyes (Fig. 2a). In contrast, under light exposure, the photodynamic bactericidal performance of the dyes demonstrated an S-shaped growth with increasing dye concentration. Significant differences in the photobiocidal performance were observed based on the type of dye. The concentrations of CV, RB, TBO, and MB required to reach the detection limit (~7.4 log reduction) were approximately 10, 12.5, 0.5, and 2.5 μM, respectively. Although the photobiocidal performance of dyes, which is affected by the wavelength of the irradiated light, may vary depending on the type of light used, we did not consider the differences in the irradiated light wavelengths and used general indoor lighting of various wavelengths to compare the photobiocidal performance of dyes under the same conditions (Fig. 1h). Thus, to optimize the photobiocidal performance of dyes, further studies are necessary.

Figure 2b shows the antibacterial performance of the dyes against *S. epidermidis* (associated with various skin-related diseases), chosen as the target Gram-positive bacterium. Compared to *E. coli*, relatively low concentrations of dye (0.1–0.85 μM)

were required to reach the limit of detection (LOD; ~6.2 log reduction) under light conditions, and the difference in the corresponding concentrations across dye types was similar. Furthermore, unlike when tested for *E. coli*, CV inactivated *S. epidermidis* up to the LoD at 100 μM under dark conditions. However, only 10 μM of CV was needed under light exposure to reach LoD. High RB, MB, and TBO concentrations also exhibited significant inactivation activity for *S. epidermidis* under dark conditions (~2.2 log reduction). These results indicate that *E. coli* is more resistant to photobiocidal reactions compared to *S. epidermidis*, consistent with previous studies on the antimicrobial performance of dyes against Gram-positive and Gram-negative bacteria. Such species-dependent differences in the antibacterial effectiveness of dyes stem from variations in the cell structure of Gram-negative/positive bacteria. (Dahl et al., 1988; Malik et al., 1992; Usacheva et al., 2001). The outer wall of the Gram-positive species, located on the exterior of the cytoplasmic membrane, has a relatively porous structure that allows for the passage of nutrients and PSs. By contrast, Gram-negative bacteria possess a highly structured outer membrane with a thickness of approximately 10–15 nm. This membrane acts as a barrier to the penetration of PSs and photoreactive species (Nikaido, 1994; Maisch et al., 2004). This limited penetration is evident in the differential inactivation performance observed under dark conditions. Furthermore, the presence of carotenoids in the intracellular content of the Gram-negative bacteria increased their resistance against photoinactivation.

Figures 2c and 2d show the antiviral performance of different dyes against phages MS2 and phi 6 according to dye concentrations. Phage MS2 was selected as the target virus because it is frequently used as a surrogate for human enteric viruses owing to their similar size and morphology (Kamimoto et al., 2014). In addition, phage phi 6 is widely employed as a surrogate for highly pathogenic enveloped viruses, such as SARS-CoV-2, Ebola, and influenza, in various biotechnological applications (Jeong et al., 2023; Sorinolu et al., 2023). Although phage phi 6 belongs to a different Baltimore group (group III) than SARS-CoV-2 (group IV), they share structural and morphological similarities, including a round shape and lipid envelope. Under light conditions, compared to the bacteria test, the minimum dye concentration required to reach the bacteriophage detection limit was lower. These observations are consistent with previous studies demonstrating that viral particles are more susceptible to photosensitization than bacteria (Andrea et al., 2015; Svyatchenko et al., 2021;

Wagner et al., 2005). Both TBO and MB exhibited outstanding photobiocidal performance against bacteria and viruses, maintaining consistent minimum concentrations required to reach the LOD, despite variation in the virus types. By contrast, the photobiocidal efficacy of CV and RB varied depending on the type of virus. (Andrea et al., 2015). The photobiocidal performance of the dyes was significantly reduced in the case of phage MS2 compared to phi 6. Phages MS2 and phi 6 have similarities, such as positive-sense and single-stranded RNA viruses. However, their structures are significantly different: phage MS2 has a non-enveloped structure while phage phi 6 has an enveloped structure. Owing to its non-enveloped nature, phage MS2 is more resistant to chemical disinfectants and can withstand environmental stressors such as temperature variation, desiccation, and osmotic pressure (Costa et al., 2012; Desai et al., 2023). These differences were more noticeable under dark conditions. Even at high concentrations, no significant inactivation was observed for phage MS2 up to a concentration of ~500 μM for all dyes (Fig. 2c), while CV and RB reached the LoD for phage phi 6 when the concentration was >100 μM (Fig. 2d).

The photobiocidal performances were highly dependent on the types of dye and the types of microorganisms. Under light exposure, the dye molecules absorb photons and generate the ROS, which induces cell death (Fig. 3a). The efficacy of the dyes in terms of photodynamic inactivation performance depends on the yield of the ROS production (Wainwright, 1998; Chen et al., 2010). To better understand the relationship between the ROS generation and photobiocidal performances, we investigated the time-resolved photoluminescence (PL) decay for the selected dyes (Fig. 3b). The PL average lifetime represents the mean duration time between the excitation and return of the excited singlet state (S_1) to the ground state (S_o) through fluorescence (green line in Fig. 3a), indicating the recombination of the photogenerated electron–hole pairs (Heo et al., 2022; Sen et al., 2022a). The calculated PL average lifetimes for RB, CV, TBO, and MB were 0.176, 0.247, 0.363, and 0.419 ns, respectively. Longer PL average lifetimes facilitate increased recombination of the electron–hole pairs before transitioning into the excited triplet states (T_1). Consequently, this phenomenon can inhibit the formation of T_1 state (black squiggly line in Fig. 3a) (Heo et al., 2022), which are involved in the ROS generation. To further understand the ROS generation, we evaluated the autolysis of the dye as a function of light intensity. Upon exposure to light, the dyes generate ROS, which can lead to the self-degradation of the dyes (Sen

et al., 2022b). The self-degradation rate of the dyes under light conditions can indicate the amount of ROS produced. Figures 3c and 3d show the time- and light intensity-dependent self-degradation of the dyes. Upon exposure to light, the concentration of CV showed minimal variations compared to other dyes, which experienced a significant decrease in the concentration with increasing exposure time. This suggests that CV may exhibit a limited capacity for ROS generation compared to other dyes, thereby lowering its inactivation performance (Noimark et al., 2016).

The PL average lifetime of CV was shorter than those of TBO and MB; however, its photobiocidal performance and light intensity-dependent self-degradation rate were not better. This may be attributed to the quantum yield (blue line in Fig. 3a), signifying the capacity of the dyes to produce excited electrons upon light absorption (Gandra et al., 2004). Although CV exhibited a shorter PL average lifetime compared to those of TBO and MB, its quantum yield (0.019) was significantly lower than those of the others (TBO: 0.076 and MB: 0.04). Moreover, in low-viscosity solvents (*i.e.*, CV) can rotate freely owing to the opposing effects due to the arrangement of the aryl rings, thereby forming a propeller-like structure. This rotational freedom of the CV molecules results in the formation of a twisted intramolecular charge transfer state in the solution as opposed to intersystem crossing to the T_1 state. (Haidekker and Theodorakis, 2010). Therefore, the probability of reaching the T_1 state is diminished (Noimark et al., 2016).

RB exhibited the shortest PL average lifetime and the highest light intensity-dependent self-degradation rate (Fig. 3b), indicating a high ROS production yield. Despite its potential for high ROS generation, the disparity in the inactivation performance based on the type of microorganisms was most pronounced. RB exhibited the highest photobiocidal performance against *S. epidermidis* (0.25 μM); however, its efficacy against *E. coli* was the lowest (12.5 μM). This substantial reduction in the bactericidal performance, dependent on the bacterial strain, is associated with the charge of the dye (Spagnul et al., 2015). The surface charges of the bacteria were consistently negative, except under pH conditions below 2 (Martinez et al., 2002). The outer membranes of the Gram-negative bacteria were more negatively charged owing to the presence of peptidoglycan, which is rich in carboxyl and amino groups, attracting cationic PSs and repelling the anionic ones. Wilhelm et al. reported that the negative charge density of the outer membrane of the Gram-

negative *E. coli* (8.7 ± 1.7 nm^{-2}) was approximately seven times higher than that of the Gram-positive *Lactobacillus Rhamnoses* (1.2 ± 0.2 nm^{-2}) (Wilhelm et al., 2021). Thus, it was inherently difficult for RB, an anionic dye, to attach to the outer wall of Gram-negative bacteria. In addition, this diminished photobiocidal performance due to attachment issues was also observed in viruses. The viruses also possessed a negative surface charge, which resulted in poor attachment of RB; thereby, hindering the attachment of RB and decreasing its virucidal performance. The difference in the virucidal efficacy of RB compared to those of TBO or MB was minor in the case of the less-resistant phage phi 6. However, against the highly charged and resistant phage MS2, RB exhibited approximately 10-fold lower virucidal performance than TBO or MB. These findings emphasize that the performance of the PS itself is critical and that the relationship between the microorganism and the PS is a significant factor for PACT.

Considering the differences in the microbial structures, it is noteworthy that the photobiocidal efficacies of TBO and MB were similar. For the virucidal test, TBO and MB required a concentration of only 0.05 μM to reach the LoD, regardless of virus type. In addition, both MB and TBO exhibited effective bactericidal performance against both bacteria. These dyes could undergo Type-I and Type-II photoreactions (Wiehe et al., 2019); the damage induced by Type-I and Type-II photoreactions is not confined to DNA/RNA, i.e., phenothiazine dyes can also damage viral surface structures such as proteins.

Conclusion

This study provides meaningful insights by presenting a comparative analysis of the photobiocidal performance of VLA dyes against various microorganisms. Although all dyes demonstrated excellent photobiocidal activities compared to under the dark condition, we focused on elucidating the subtle differences in these activities. Owing to differences in the biological structure between Gram-negative and Gram-positive bacteria, Gram-negative *E. coli* exhibited higher resistance to the photobiocidal reactions than the Gram-positive *S. epidermidis*. Similar to the bacteria, in viruses, the differences in the structures led to differences in the resistance to the photochemical reaction. The non-enveloped structure of phage MS2 is more resistant to photobiocidal reaction compared to the enveloped structure of phage phi 6.

In our study, time-resolved PL decay measurements and light intensity-dependent self-degradation rate assessments indicated the possibility of the highest ROS production yield of RB, leading to the expectation of superior photobiocidal activity. However, the photobiocidal activity of RB changed dramatically according to the surface charge of the microbes. TBO was least dependent on microbial types. TBO required for bactericidal and virucidal performances to reach LoD were 0.5 and 0.05 μM, respectively. These findings highlight the importance of examining the relationship between the microbes and PS to optimize the photobiocidal performance by appropriately selecting PACT-driving agents based on the target microbes. While this study established the relationship between PS and two bacteria and two viruses, future studies are required to confirm the photobiocidal reactions to various microorganisms, including fungi and AMR germs. Furthermore, although this study provides information on the minimum concentrations at which the photobiocidal activity occurs, further research is required on the risk of human cell damage due to ROS generation under high concentrations of the PS. . Nevertheless, our results could serve as a foundation for developing various antibacterial and antiviral technologies using VLA organic dyes.

Author contribution

Jae Hak Shin: Conceptualization, Methodology, Visualization, Writing. **Sang Bin Jeong:** Investigation, Visualization, Writing. **In Ho Kim:** Data curation, Methodology. **Seung Yeon Lee:** Data curation, Methodology. **Gi Byoung Hwang:** Investigation. **Inyong Park:** Investigation. **Ki Joon Heo:** Investigation, Supervision, Writing. **Jae Hee Jung:** Conceptualization, Supervision, Funding acquisition, Project administration Writing

Declaration of competing interest

The authors declare no competing financial interest.

Acknowledgements

This work was supported by the National Research Foundation of Korea (NRF) grant

funded by the Korea government (MSIT) (2022R1A2B5B02001231; RS-2023-00213266). It was also partly supported by the Basic Research Fund from the Korea Institute of Machinery and Materials (NK231A) and by the "Regional Innovation Strategy (RIS)" through NRF funded by the Ministry of Education (MOE)(2021RIS-002).

Reference

Andrea, C., Duygu, E., Rohan, V.T., Nitin, N., 2015. Antimicrobial effect of photosensitized Rose Bengal on bacteria and viruses in model wash water. Food. Bioproc. Tech. 9, 441-451. https://doi.org/10.1007/s11947-015-1631-8

Castano, A.P., Demidova, T.N., Hamblin, M.R., 2004. Mechanisms in photodynamic therapy: part one-photosensitizers, photochemistry and cellular localization. Photodiagnosis Photodyn. Ther. 1(4), 279–293. https://doi.org/10.1016/S1572-1000(05)00007-4

Chen, J., Cesario, T.C., Rentzepis, P.M., 2010. Time resolved spectroscopic studies of methylene blue and phenothiazine derivatives used for bacteria inactivation. Chem. Phys. Lett. 498, 81–85. https://doi.org/10.1016/j.cplett.2010.08.042

Costa, L., Tomé, J.P.C., Neves, M.G.P.M.S., Tomé, A.C., Cavaleiro, J.A.S., Cunha, Â., Faustino, M.A.F., Almeida, A., 2012. Susceptibility of non-enveloped DNA- and RNA-type viruses to photodynamic inactivation. Photochem. Photobiol. Sci. 11, 1520-1523. https://doi.org/10.1039/c2pp25156f

Dahl, T.A., Robert Midden, W., Neckers, D.C., 1988. Comparison of photodynamic action by Rose Bengal in Gram-positive and Gram negative bacteria. Photochem. Photobiol. 48, 607–612. https://doi.org/10.1111/j.1751-1097.1988.tb02870.x

Daniell, M.D., Hill, J.S., 1991. A history of photodynamic therapy. Amz. J. Surg. 61, 340–348. https://doi.org/10.1111/J.1445-2197.1991.TB00230.X

Derosa, M.C., Crutchley, R.J., 2002. Photosensitized singlet oxygen and its applications. Coord. Chem. Rev. 233, 351–371. https://doi.org/10.1016/S0010-8545(02)00034-6

Desai, G., Ramachandran, G., Goldman, E., Esposito, W., Galione, A., Lal, A., Choueiri, T.K., Fay, A., Jordan, W., Schaffner, D.W., Caravanos, J., Grignard, E., Mainelis, G., 2023. Efficacy of Grignard Pure to inactivate airborne phage MS2, a common SARS-CoV-2 surrogate. Environ. Sci. Technol. 57(10), 4231-4240. https://doi.org/10.1021/acs.est.2c08632

Gandra, N., Frank, A.T., Le Gendre, O., Sawwan, N., Aebisher, D., Liebman, J.F., Houk, K.N., Greer, A., Gao, R., 2004. Possible singlet oxygen generation from the photolysis of indigo dyes in methanol, DMSO, water, and ionic liquid, 1-butyl-3-methylimidazolium tetrafluoroborate. J. Biol. Chem. 279, 18521–18525. https://doi.org/10.1016/j.tet.2006.08.095

Haidekker, M.A., Theodorakis, E.A., 2010. Environment-sensitive behavior of fluorescent molecular rotors. J. Biol. Eng. 4(11). 1-14.

https://doi.org/10.1186/1754-1611-4-11

Hamblin, M.R., Hasan, T., 2004. Photodynamic therapy: a new antimicrobial approach to infectious disease? Photochem. Photobiol. Sci. 3(5), 436-450. https://doi.org/10.1039/b311900a

Heo, K.J., Lee, D.U., Shin, J.H., Park, J., Lee, B.J., Shin, J., Jeong, S.B, Hwang, G.B., MacRobert, A.J., Parkin, I.P., Jung, J.H., Choi, D.Y., 2022. Transparent, Robust, and Photochemical Antibacterial Surface Based on Hydrogen Bonding between a Si-Al and Cationic Dye. ACS Appl. Mater. Interf. 14, 53285–53297. https://doi.org/10.1021/acsami.2c16071

Nikaido, H., 1994. Prevention of drug access to bacterial targets: Permeability barriers and active efflux. Science 264, 382–388. https://doi.org/10.1126/science.8153625

Jeong, S.B., Shin, J.H., Kim, S.W., Seo, S.C., Jung, J.H., 2023. Performance evaluation of an electrostatic precipitator with a copper plate using an aerosolized SARS-CoV-2 surrogate (bacteriophage phi 6). Environ. Technol. Innov. 30, 103124:1-11. https://doi.org/10.1016/j.eti.2023.103124

Kamimoto, M., Nakai, Y., Tsuji, T., Shimamoto, T., Shimamoto, T., 2014. Antiviral effects of persimmon extract on human norovirus and its surrogate, bacteriophage MS2. J. Food. Sci. 79, M941–M946. https://doi.org/10.1111/1750-3841.12462

Klausen, M., Ucuncu, M., Bradley, M., 2020. Design of photosensitizing agents for targeted antimicrobial photodynamic therapy. Molecules 25, 5239:1-30. https://doi.org/10.3390/MOLECULES25225239

Kumar, S., 2021. Antimicrobial resistance: a top ten global public health threat. EClinicalMedicine 41, 101221. https://doi.org/10.1016/j.eclinm.2021.101221

O'Neill, J. 2016. Tackling drug-resistant infections globally: final report and recommendations, Review on Antimicrobial Resistance, Government of the United Kingdom.

Maisch, T., Szeimies, R.-M., Jori, G., Abels, C., 2004. Antibacterial photodynamic therapy in dermatology. Photochem. Photobiol. Sci. 3, 907–917. https://doi.org/10.1039/b407622b

Malik, Z., Ladan, H., Nitzan, Y., 1992, undefined, 1992. Photodynamic inactivation of Gram-negative bacteria: problems and possible solutions. J. Photochem. Photobiol. B. 14, 262–266. https://doi.org/10.1016/1011-1344(92)85104-3

Martinez, R.E., Smith, D.S., Kulczycki, E., Ferris, F.G., 2002. Determination of intrinsic bacterial surface acidity constants using a Donnan shell model and a

continuous pKa distribution method. J. Colloid Interf. Sci. 253, 130–139. https://doi.org/10.1006/jcis.2002.8541

Murray, C.J.L., Ikuta, K.S., Sharara, F., Swetschinski, L., Aguilar, G.R., et al., 2022. Global burden of bacterial antimicrobial resistance in 2019: a systematic analysis. Lancet 399, 629–655. https://doi.org/10.1016/S0140-6736(21)02724-0

Noimark, S., Salvadori, E., Gómez-Bombarelli, R., Macrobert, A.J., Parkin, I.P., Kay, C.W.M., 2016. Comparative study of singlet oxygen production by photosensitiser dyes encapsulated in silicone: towards rational design of anti-microbial surfaces. Phys. Chem. Chem. Phys. 18, 28101-28109. https://doi.org/10.1039/c6cp02529c

Rolim, J.P.M.L., de-Melo, M.A.S., Guedes, S.F., Albuquerque-Filho, F.B., de Souza, J.R., Nogueira, N.A.P., Zanin, I.C.J., Rodrigues, L.K.A., 2012. The antimicrobial activity of photodynamic therapy against *Streptococcus mutans* using different photosensitizers. J. Photochem. Photobiol. B. 106, 40-46. https://doi.org/10.1016/j.jphotobiol.2011.10.001

Sen, P., Soy, R., Mgidlana, S., Mack, J., Nyokong, T., 2022a. Light-driven antimicrobial therapy of palladium porphyrins and their chitosan immobilization derivatives and their photophysical-chemical properties. Dyes Pigm. 203, 110313:1-11. https://doi.org/10.1016/j.dyepig.2022.110313

Sen, S., Das, C., Ghosh, N.N., Baildya, N., Bhattacharya, S., Khan, M.A., Sillanpää, M., Biswas, G., 2022b. Is degradation of dyes even possible without using photocatalysts? – a detailed comparative study. RSC Adv. 12, 34335–34345. https://doi.org/10.1039/D2RA05779D

Soria-Lozano, P., Gilaberte, Y., Paz-Cristobal, M., Pérez-Artiaga, L., Lampaya-Pérez, V., Aporta, J., Pérez-Laguna, V., García-Luque, I., Revillo, M., Rezusta, A., 2015. In vitro effect photodynamic therapy with differents photosensitizers on cariogenic microorganisms. BMC Microbiol. 15, 187:1-8. https://doi.org/10.1186/S12866-015-0524-3

Sorinolu, A.J., Mamun, M.M., Vadarevu, H., Vivero-Escoto, J.L., Vejerano, E.P., Munir, M., 2023. Antiviral activity of nano-monocaprin against Phi6 as a surrogate for SARS-CoV-2. Int. Microbiol. 26, 379–387. https://doi.org/10.1007/s10123-022-00300-6

Spagnul, C., Turner, L.C., Boyle, R.W., 2015. Immobilized photosensitizers for antimicrobial applications. J. Photochem. Photobiol. B. 150, 11-30. https://doi.org/10.1016/j.jphotobiol.2015.04.021

Svyatchenko, V.A., Nikonov, S.D., Mayorov, A.P., Gelfond, M.L., Loktev, V.B., 2021. Antiviral photodynamic therapy: Inactivation and inhibition of SARS-CoV-2 in

vitro using Methylene Blue and Radachlorin. Photodiagnosis Photodyn. Ther. 33, 102112:1-5. https://doi.org/10.1016/J.PDPDT.2020.102112

Usacheva, M.N., Teichert, M.C., Biel, M.A., 2001. Comparison of the methylene blue and toluidine blue photobactericidal efficacy against Gram-positive and Gram-negative microorganisms. Lasers Surg. Med. 29, 165–173. https://doi.org/10.1002/lsm.1105

Vilela, S.F.G., Junqueira, J.C., Barbosa, J.O., Majewski, M., Munin, E., Jorge, A.O.C., 2012. Photodynamic inactivation of *Staphylococcus aureus* and *Escherichia coli* biofilms by malachite green and phenothiazine dyes: An *in vitro* study. Arch. Oral Biol. 57, 704–710. https://doi.org/10.1016/j.archoralbio.2011.12.002

Wagner, S.J., Skripchenko, A., Donnelly, D.J., Ramaswamy, K., Detty, M.R., 2005. Chalcogenoxanthylium photosensitizers for the photodynamic purging of blood-borne viral and bacterial pathogens. Bioorg. Med. Chem. 13(21), 5927-5935 https://doi.org/10.1016/j.bmc.2005.07.035

Wainwright, M., 1998. Photodynamic antimicrobial chemotherapy (PACT). J. Antimicrob. Chemother. 42, 13–28. https://doi.org/10.1093/jac/42.1.13

Wiehe, A., O'brien, J.M., Senge, M.O., 2019. Trends and targets in antiviral phototherapy. Photochem. Photobiol. Sci. 18, 2565–2612. https://doi.org/10.1039/C9PP00211A

Wilhelm, M.J., Sharifian, M.G., Wu, T., Li, Y., Chang, C., Ma, J., Dai, H.L., 2021. Determination of bacterial surface charge density via saturation of adsorbed ions. Biophys. J. 120(12), 2461–2470. https://doi.org/10.1016/j.bpj.2021.04.018

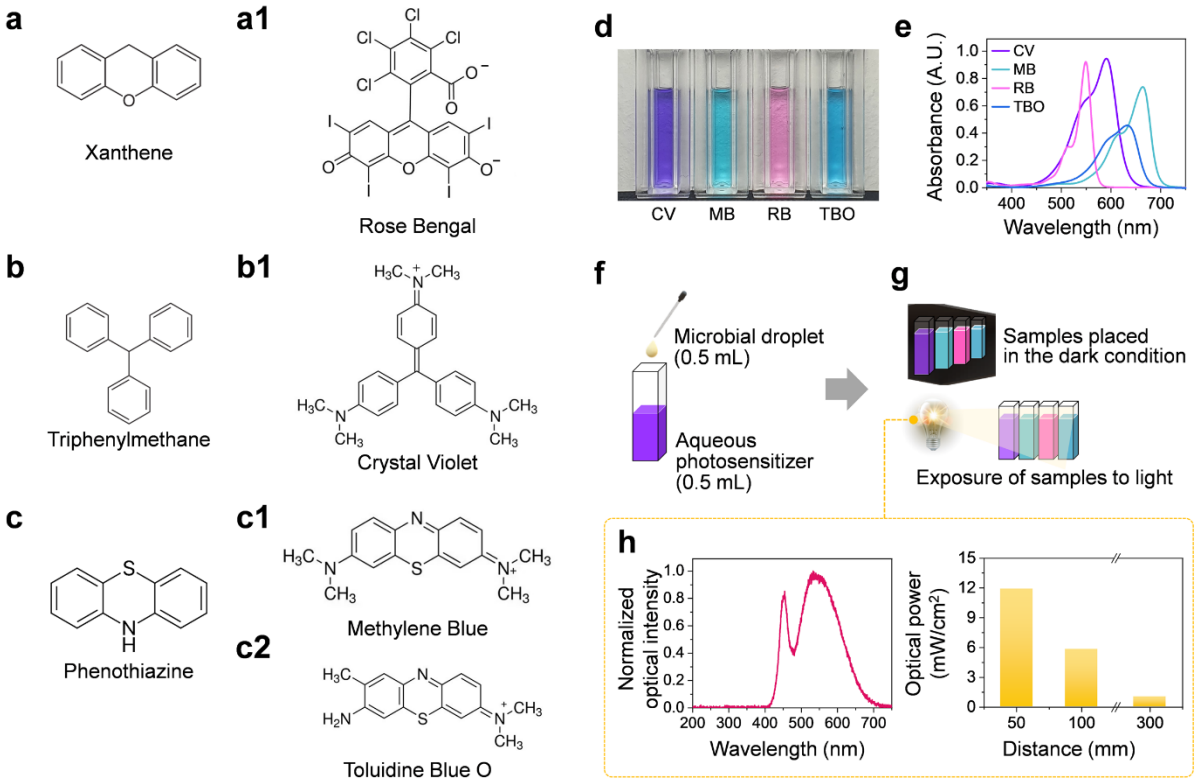

Figure 1. Chemical structures of (a) xanthene, (b) triphenylmethane, and (c) phenothiazine dye. (d) A photo of the VLA dyes in cuvettes at a concentration of 10 μM. (e) UV–Vis absorbance spectra of the VLA dyes (10 μM). Schematics of (f) the photobiocidal test procedure and (g) light exposure test method. (h) Lamp spectrum and optical power according to distance.

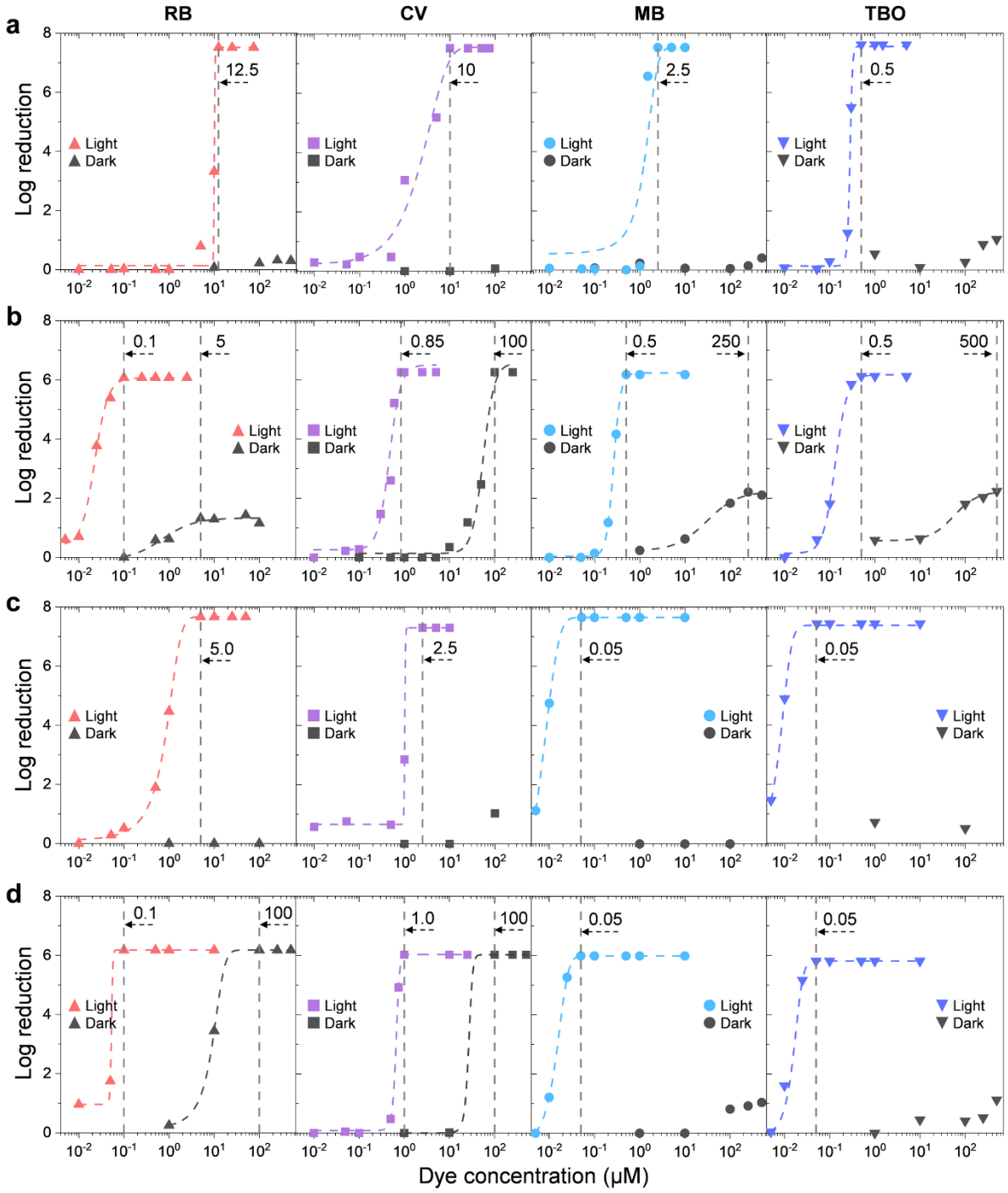

Figure 2. Photochemical inactivation performances of different dyes used in this study against (a) *E. coli*, (b) *S. epidermidis*, (c) phage MS2, and (d) phage phi 6.

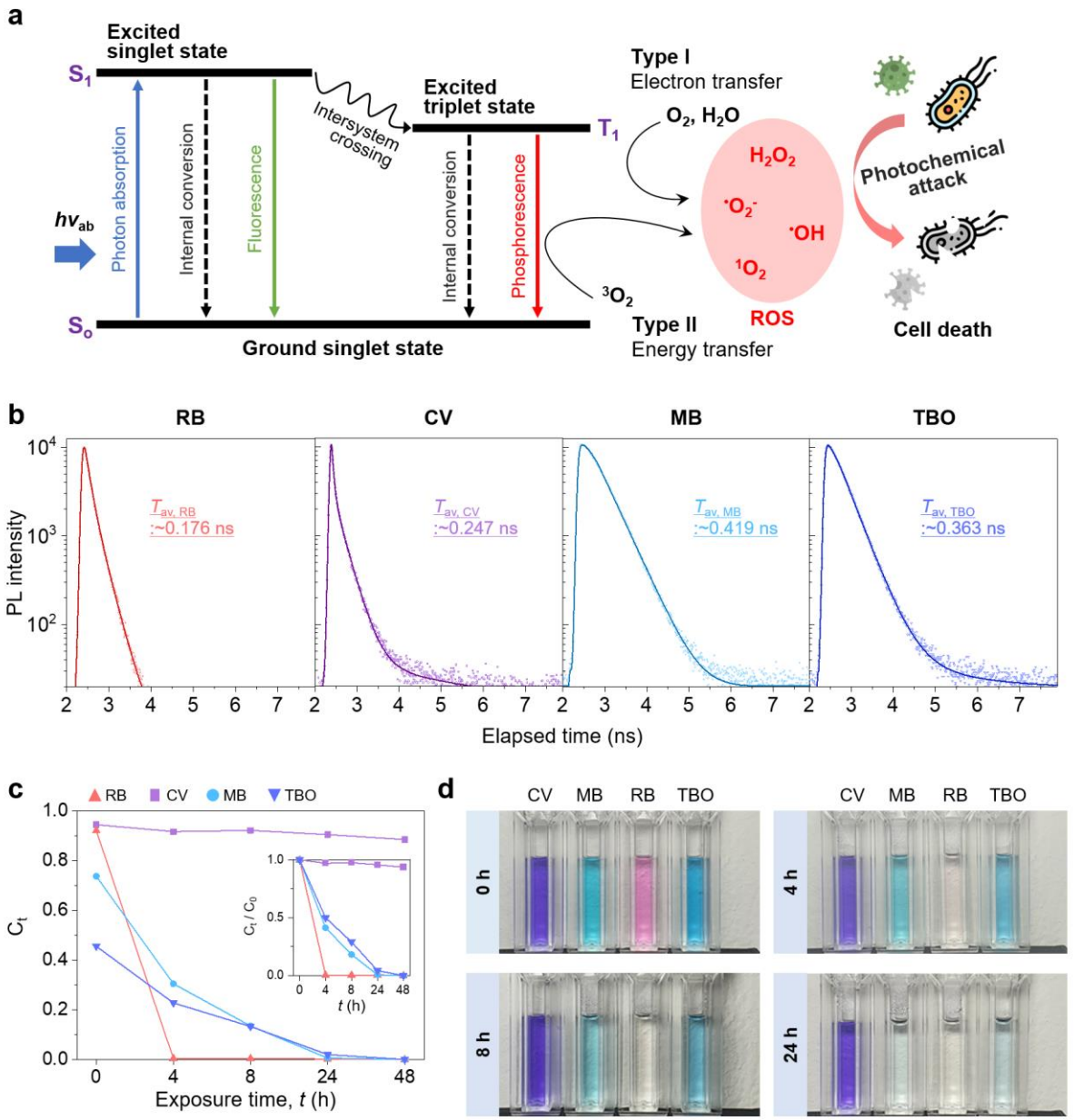

Figure 3. Photoreaction characterization of dyes. (a) Jablonski diagram. (b) Time-resolved PL decay of RB, CV, MB, and TBO. (c) Absorbance changes in dyes with respect to the light exposure time. C_t and C_0 are the absorbance of dye at peak point of the exposure time and initial time, respectively. The Inset image shows the normalized absorbance changes according to elapsed time. (d) Digital images of dyes as function of light exposure time.